

University of Wisconsin - Madison

MADPH-95-909
RAL-TR-95-063
hep-ph/9511459
November 1995

Top pair production with an extra gluon at the Tevatron

V. Barger^a, P.G. Mercadante^a and R.J.N. Phillips^b

^a*Physics Department, University of Wisconsin, Madison, WI 53706, USA*

^b*Rutherford Appleton Laboratory, Chilton, Didcot, Oxon OX11 0QX, UK*

Abstract

We calculate top pair production and decay at the Tevatron $p\bar{p}$ collider, with the emission of an extra gluon, and study the corresponding $W + 5$ jet top signals including full spin correlations in the $W \rightarrow \ell\nu$ leptonic and $W \rightarrow jj$ hadronic decays. We study the feasibility of reconstructing $W + 5$ jet top events with a single b -tag, including realistic energy resolution. Our suggested basic procedure based on kinematic fitting achieves about 74% reconstruction efficiency, with 74% of the reconstructed events correctly classified (purity); this improves to 82% efficiency with 77% purity in double- b -tagged events. We suggest possible refinements, based on virtuality criteria, that give higher purity at the cost of lower reconstruction efficiency.

arXiv:hep-ph/9511459v1 29 Nov 1995

Now that top quark signals have been seen at the Tevatron, in both the dilepton+jets and single-lepton + 4jets channels and by both the CDF and D0 collaborations [1,2], it is interesting to explore other channels where top signals may be found. The underlying parton mechanism for producing these signals at the Tevatron energy is dominantly

$$q + \bar{q} \rightarrow t + \bar{t} \rightarrow (bW^+)(\bar{b}W^-), \quad (1)$$

with either one or both of the W bosons decaying leptonically: $W \rightarrow \ell\nu$ ($\ell = e, \mu$). It is important to tag one or more of the b -jets, by a displaced vertex or by a lepton from b -decay, in order to establish the signal and discriminate against background. For determining the top quark mass, it is preferable to study the $(W \rightarrow \ell\nu) + 4$ jets channels, where one of the W -bosons decays hadronically ($W \rightarrow jj$) and a suitably chosen three-jet combination has invariant mass $m(bjj) \simeq m_t$, avoiding problems with invisible neutrinos. The principal background in the $W + 4$ jets channel comes from the electroweak production of a single W -boson plus four QCD jets [3], but with the usual acceptance cuts and b -tagging this background is much smaller than the signal.

In high- Q^2 processes like top pair production, it is not uncommon that additional hard QCD radiation (typically a gluon) will be emitted, viz

$$q + \bar{q} \rightarrow (bW^+)(\bar{b}W^-)g. \quad (2)$$

Here the gluon can be radiated either from the incident quarks, or from the produced top quarks before they decay, or from subsequent top decays into bW , and complete calculations have recently been performed [4] exploiting the MADGRAPH program [5]. These improve on previous calculations that omitted radiation from top decay [6]; the new results coherently combine the effects of radiation during both production and decay processes, together with their interference. The radiation of gluons from the color-disconnected process of hadronic W -decay ($W \rightarrow jj$) can be ignored here, since the hadronically decaying W is identified experimentally as a dijet with invariant mass $m(jj) \simeq M_W$. In the five-jet channel, it seems very likely that the background from $W + 5$ QCD jets will also be small compared to the signal, after b -tagging.

Basic reconstruction of single-tagged events

To make use of the resulting $(W \rightarrow \ell\nu) + 5$ jet final states in the study of top signals, some criteria must be established to distinguish the gluon jet from the other jets. One b -jet is identified by tagging. The $W \rightarrow jj$ dijet is identified by its invariant mass,

$m(jj) \simeq M_W$ (it is extremely unlikely that either of these is a b -jet). The remaining two jets are presumably from one gluon and one b -quark; we propose to identify the gluon with the jet of lower transverse momentum p_T , since the b -jets from $t \rightarrow bW$ have typically high p_T with a Jacobian peak at $p_T \simeq (m_t^2 - M_W^2)/(2m_t) \simeq 70$ GeV in the t -restframe. Finally the $W \rightarrow \ell\nu$ decay can be reconstructed within a two-fold ambiguity using the invariant mass constraint $m(\ell\nu) \simeq M_W$, when we attribute the missing transverse momentum \cancel{p}_T in the event to the neutrino ($\cancel{p}_T = \mathbf{p}_T(\nu)$). There are now twelve different configurations, in which a $W + 5$ jet event can be interpreted as top pair production and decay, with a gluon emitted either in the initial production or in the final decay process:

$$\text{Class A: } g(t \rightarrow W_{\ell\nu}b)(t \rightarrow W_{jj}b), \quad (3)$$

$$\text{Class B: } (t \rightarrow W_{\ell\nu}bg)(t \rightarrow W_{jj}b), \quad (4)$$

$$\text{Class C: } (t \rightarrow W_{\ell\nu}b)(t \rightarrow W_{jj}bg). \quad (5)$$

There are four configurations in each class, corresponding to two $W \rightarrow \ell\nu$ solutions and two different ways to pair the b -quarks with W -bosons. Although we evaluate all the diagrams in each event, Class A is well represented by diagrams a,b,e,f,g shown in Figure 1, Class B by d,f and Class C by c,e (in the case of $W^+ \rightarrow \ell^+\nu$ leptonic decay). We note that gluon emission from a top quark can contribute to Class A or B or C. The underlying idea for event reconstruction is that events are most likely to occur in regions of phase space where one class of Feynman diagrams has both a top propagator and an antitop propagator near the mass shell, and are unlikely otherwise; the near-shell propagators define the event class. Thus almost all events fall into one of the Classes A,B,C, although a very small fraction may defy this classification (e.g. one top may decay far off-shell).

Lepton-tagging of the b -jet would distinguish b from \bar{b} and hence reduce the number of competing configurations to six (two in each class), improving the prospects for a correct reconstruction. Our analysis neglects this positive feature, implicitly assuming vertex-tagging; however, we also neglect for simplicity the negative effects of possible mistagging (illustrated in Ref. [7]).

Our procedure is first to identify the gluon and other jets as indicated above (with $W \rightarrow jj$ the best fit of untagged jet pairs), and then to evaluate the invariant masses m_1, m_2 of the two ‘‘top’’ candidate clusters in each configuration, and to assign a closeness-

of-fit parameter

$$F = (m_1 - m_t)^2 + (m_2 - m_t)^2, \quad (6)$$

assuming that the top mass m_t will have been accurately determined from $W + 4$ -jet events. The configuration with lowest F is designated the best fit ; it assigns the event to Class A, B, or C, gives the reconstruction of all momenta, and fixes which jet is b and which is \bar{b} . We require $F_{\min} < 500 \text{ GeV}^2$ for an acceptable fit ($\sqrt{F_{\min}/2} = 16 \text{ GeV}$), otherwise the reconstruction is deemed to fail.

Tests with Monte Carlo events

We have tested this procedure with Monte Carlo ($W \rightarrow \ell\nu$) + 5 jet events generated by the MADGRAPH program [5], using the observed top mass $m_t = 174 \text{ GeV}$ [1,2] and calculated decay width $\Gamma_t = 1.53 \text{ GeV}$. To simulate detector energy resolution we add realistic gaussian smearing:

$$\Delta E/E = 0.15/\sqrt{E/\text{GeV}} \quad (\text{for leptons}), \quad (7)$$

$$\Delta E/E = 0.8/\sqrt{E/\text{GeV}} \quad (\text{for quarks}). \quad (8)$$

We also make the following acceptance cuts, broadly typical of Tevatron top analyses:

$$\begin{aligned} p_T(\ell) &> 20 \text{ GeV} & |\eta(\ell)| &< 2.5 \\ p_T(j) &> 10 \text{ GeV} & |\eta(j)| &< 2.5 \\ \Delta R(\ell j) &> 0.4 & \Delta R(jj) &> 0.4 \\ \cancel{p}_T &> 25 \text{ GeV} \end{aligned} \quad (9)$$

where $\eta = \ln \tan(\theta/2)$ is pseudorapidity, $(\Delta R)^2 = (\Delta\eta)^2 + (\Delta\phi)^2$ measures angular separation, while θ and ϕ are the usual polar and azimuthal angles with respect to the beam. These cuts are applied at the parton level, interpreting quarks and gluons as jets.

In the absence of smearing, we find that our procedure correctly reconstructs about 95% of single- b -tagged events that pass the acceptance cuts; misreconstructions and failures occur in the 5% of events where the gluon has higher p_T than the untagged b -jet (and is therefore incorrectly identified). There are very few events where the top-quark propagators are so far off-shell that they alone give $F_{\min} > 500 \text{ GeV}^2$.

For smeared Monte Carlo events, the success of our reconstruction procedure (after acceptance cuts) is shown in Table 1. The first two columns give the percentage of events in true classes, determined from event kinematics before smearing. Columns 3–6 show

Table 1: Basic reconstruction for smeared single- b -tagged events after cuts.

True class and percent			Percentage in reconstructed classes			
			A	B	C	Fail
A	59.7	\Rightarrow	32.5	4.8	4.5	17.9
B	20.2	\Rightarrow	4.1	9.9	2.0	4.2
C	20.1	\Rightarrow	2.5	1.6	12.1	3.9

the corresponding percentages that are reconstructed in Classes A–C or fail (because $F_{\min} > 500 \text{ GeV}^2$). Failures and misreconstructions typically arise in events where, after smearing, the wrong pair of jets gives the best fit to $W \rightarrow jj$, or the gluon has higher p_T than the untagged b -jet.

These results show that 55% of events passing the cuts are correctly reconstructed in Class A, B or C, while 19% are incorrectly reconstructed (in the wrong class) and 26% fail to reconstruct; in other words, our procedure has 74% reconstruction efficiency and 74% purity (correctness of classification), albeit with different degrees of purity (83%,61%,65%) in different reconstructed classes (A,B,C). We surmise that a similar success rate would be achieved with real data.

It is interesting to investigate how well such reconstructed events reproduce the correct dynamical distributions for gluons emitted before (Class A) or during (Classes B,C) the top quark decay, i.e. whether the reconstruction procedure introduces significant biases. Figure 2 shows distributions versus gluon transverse momentum $p_T(g)$ for Class A,B,C events; solid histograms represent true unsmeared events while dashed histograms compare the behaviour of reconstructed smeared events (normalized to the same area). The solid/dashed discrepancies can be qualitatively understood as follows. Class A events with soft gluons (hence small p_T) can rather easily fake B or C after smearing, because such gluons affect invariant masses rather little, so we lose A and gain B,C events at small $p_T(g)$. There is a flow the other way, too, which apparently wins out at larger $p_T(g)$. We see that the true A,B,C $p_T(g)$ -dependences are very similar (solid histograms), but the misidentification probabilities change with $p_T(g)$ and the dashed histograms are rather different.

Similarly, Fig. 3 compares true and reconstructed distributions of the separation $\Delta R(gb)$ between the gluon jet and its associated b -jet in Class B and C events. True

events show the expected sharp peak at small ΔR (cut off by our acceptance criteria at $\Delta R = 0.4$), due to the propagator of the off-shell b^* -quark in the radiation process $b^* \rightarrow bg$. Reconstructed histograms, however, contain 20-30% backgrounds of misidentified events (mostly from Class A) with different dynamical origins that give no such peak.

Figure 4 compares true and reconstructed distributions versus gluon energy $E(g)$ in the parent top rest-frame, for Class B and C events. The same 20–30% backgrounds are present here too, but apparently have much the same $E(g)$ -dependence as the true signal.

Refined reconstruction for single-tagged events

The results above show that many misreconstructed events do not have the expected close correlation with the beam line (Class A, see Fig. 2(a)) or with the associated b -jet (Classes B and C, see Fig. 3). We have therefore investigated ways to incorporate such correlations into the reconstruction procedure; it seems that the best-motivated way is to introduce the relevant virtuality in each configuration, as follows. For Class A, we consider the virtuality $[p(q^*)]^2 = [p(q) - p(g)]^2 = -2p(q).p(g)$ of the off-shell quark q^* that would be recoiling against a gluon g radiated from an initial quark or anti-quark q ; we choose the lowest of the two possible values corresponding to the incident quark and anti-quark; this quantity is ≤ 0 and vanishes at the q^* -propagator pole. For Classes B and C, we consider the virtuality $[p(b^*)]^2 - m_b^2 = [p(b) + p(g)]^2 - m_b^2 = 2p(b).p(g)$ of the off-shell b^* -quark that would be radiating the gluon in these configurations; this quantity is ≥ 0 and vanishes at the b^* -propagator pole. Clearly, a small virtuality implies a large matrix element and hence a large likelihood that the gluon was emitted in the corresponding configuration; this suggests minimum-virtuality as an additional criterion in choosing the best fit.

We note, incidentally, that minimum-virtuality alone cannot select a unique configuration in our analysis, since each B-type configuration has the same b^* -virtuality as a C-type configuration where the (b, W) pairings are interchanged; similarly, each A-type configuration has the same q^* -virtuality as another A-type with (b, W) pairings reversed. However, in the particular case of lepton-tagging the pairings would be fixed and this degeneracy would disappear.

Accordingly, we propose to combine kinematic fitting with a minimum-virtuality cri-

Table 2: Refined reconstruction for smeared single- b -tagged events after cuts.

True class and percent			Percentage in reconstructed classes			
			A	B	C	Fail
A	59.7	\Rightarrow	15.7	2.5	2.3	39.2
B	20.2	\Rightarrow	0.5	8.3	1.1	10.4
C	20.1	\Rightarrow	0.3	1.0	9.1	9.7

terion. We now accept a given configuration as the best fit if it has both (a) the minimum F with value < 500 and (b) the minimum absolute value of virtuality, compared to all the competing configurations. The results of this more refined strategy are shown in Table 2.

These results shows a marked improvement in purity, which is now 95%, 70%, 73% in reconstructed classes A,B,C respectively (81% overall). Figure 5 presents the corresponding $\Delta R(gb)$ distributions in Class B and C events. We can see that the extra virtuality criterion brings the reconstructed distribution much closer to the true unsmeared case than previously (Fig. 3).

However, efficiency has now dropped to about 41% overall and is particularly low (34%) in events of true class A. The reason for the latter is that the different virtuality distributions are affected in quite different ways by our acceptance cuts, as we now describe. In true class B events, the relevant virtuality $[p(b^*)]^2$ peaks at zero before cuts, but this peak is removed by the $\Delta R(bg)$ cut and the remaining events have a peak around $(18 \text{ GeV})^2$ that is not much smeared by energy resolution; in contrast, the “wrong” virtualities (corresponding to incorrect A or C assignments) have broader distributions peaking near $(50\text{--}60 \text{ GeV})^2$ instead, so the minimum-virtuality criterion usually points to the correct B assignment. In true class A events, the relevant virtuality $[p(q^*)]^2$ also peaks at zero before cuts; this peak is cut out by the $p_T(g)$ and $|\eta(g)|$ cuts and the remaining distribution now vanishes below about $(20 \text{ GeV})^2$ and has a broad shape peaking around $(40\text{--}50 \text{ GeV})^2$. The “wrong” virtualities both have rather broad distributions peaking near $(60 \text{ GeV})^2$, but with wings extending down even below $(20 \text{ GeV})^2$, so the minimum-virtuality criterion now quite often points to an incorrect B or C assignment; increased conflict with the minimum-F criterion gives more failures and lower efficiency.

This overlap of right and wrong virtualities happens because the acceptance cuts

Table 3: Compromise reconstruction for smeared single- b -tagged events after cuts.

True class and percent			Percentage in reconstructed classes			
			A	B	C	Fail
A	59.7	\Rightarrow	32.5	2.5	2.3	22.4
B	20.2	\Rightarrow	4.1	8.3	1.1	6.7
C	20.1	\Rightarrow	2.5	1.0	9.1	7.5

act more harshly against small $[p(q^*)]^2$ than against small $[p(b^*)]^2$. This overlap might be reduced if there were different jet cuts, but as things stand the minimum-virtuality criterion is not particularly helpful in Class A reconstructions. We therefore propose the following compromise strategy.

Compromise strategy for single-tagged events

Since the minimum-virtuality criterion is apparently helpful in classes B and C, but not in class A reconstructions, a simple compromise strategy is to apply it only in the former cases. First select the best-fit configuration by minimizing F; if the result is Class A, accept it; if the result is Class B or C, accept it only if it also has minimum virtuality. The result of this strategy is to obtain column A from Table 1 with columns B and C from Table 2, as shown in Table 3.

This gives purity 83%, 70%, 73% in reconstructed classes A,B,C, respectively. The overall efficiency is 63%, and is roughly the same (62%, 67%, 63%) for the three true classes A,B,C.

A caveat should now be voiced. The measurement of final-state b -quark virtualities $[p(b^*)]^2 - m_b^2$ is rather straightforward, involving just the gluon-jet and associated b -jet kinematics, but initial-state virtualities $[p(q^*)]^2$ require a complete reconstruction of the event and accumulate large uncertainties (that have in fact been included in our calculations). As an alternative approach, we could choose not to rely on these q^* virtualities. There would then be no extra constraint on best fits of class A, just as in the compromise strategy above. In class B and C configurations, we could exploit the more accessible b^* virtualities by simply requiring them to be small, say less than $(50 \text{ GeV})^2$. This *ad hoc* prescription gives results very similar to Table 3.

Reconstruction pattern for double- b -tagged events

Finally it is interesting to ask how well our reconstruction strategies would work

Table 4: Basic reconstruction for smeared double- b -tagged events after cuts.

True class and percent			Percentage in reconstructed classes			
			A	B	C	Fail
A	59.7	\Rightarrow	38.7	4.6	4.5	11.9
B	20.2	\Rightarrow	4.0	11.1	1.8	3.3
C	20.1	\Rightarrow	2.4	1.4	13.6	2.7

in $W + 5$ -jet events where both b -jets have been correctly tagged. There is still some uncertainty here, after energy smearing, because the best $W \rightarrow jj$ candidates may not be the correct pair of jets, the $W \rightarrow \ell\nu$ reconstruction is still ambiguous, and we still do not know which is the b -jet and which is the \bar{b} -jet (neglecting possible lepton-tagging information as before). Table 4 shows the results of applying our basic reconstruction strategy (the same as for Table 1) to such events.

Summary

Our results may be summarized as follows.

(1) We have proposed strategies to reconstruct $(W \rightarrow \ell\nu) + 5$ -jet events, that originate from $t\bar{t}$ pair production with the emission of an extra gluon. To this end, we have introduced classes A,B,C of final states, characterized by gluon emission in the process of (A) $t\bar{t}g$ production or (B) $t \rightarrow W_{\ell\nu}bg$ decay or (C) $t \rightarrow W_{jj}bg$ decay. Although in principle these classes of event must overlap, in practice most events are expected to fall preferentially into one of these classes (with its implied kinematical constraints); however, a small fraction are expected to defy this classification and thereby to escape from reconstruction.

(2) We have tested these strategies using Monte Carlo events generated through the MADGRAPH program [5]. Since we use the full matrix elements in our calculations, the gluon can be emitted from anywhere and the amplitudes receive contributions from all three regions A,B,C. The distinction between these different regions is only made in the reconstruction procedure, where it is assumed that a single region dominates for any given event.

(3) For single- b -tagged events, distinguishing the gluon from the second b -jet by its generally lower p_T , there are twelve competing reconstructions (four in each class). Our basic strategy is to select the configuration that gives the best kinematical fit to the two

reconstructed top-quark invariant masses, i.e. minimum F subject to $F_{min} < 500$. The results, shown in Table 1, give 74% purity with 74% efficiency overall. Figures 2,3,4 compare some distributions of true and reconstructed events.

(4) A more refined strategy, where not only the top-mass discrepancies but also the implied virtuality of the radiating beam-quark (class A) or b -quark (classes B,C) are minimized simultaneously, gives 81% purity with 41% efficiency, as shown in Table 2 and Fig. 5. This strategy is rather wasteful in Class A events, however, because our acceptance cuts suppress small q^* -virtualities much more severely than small b^* -virtualities.

(5) A compromise strategy, where minimum-virtuality is required only for a best fit of Class B or C, gives better efficiency 63% (approximately the same for all classes) while still preserving reasonable purity 79%; see Table 3 and Fig. 5. If initial-state virtualities prove unworkable, this strategy can be adapted to use final-state virtualities only, with similar results.

(6) Somewhat better results are obtained in events where both b -quarks are tagged, and hence the gluon is more cleanly distinguished, as shown in Table 4. Here our basic reconstruction strategy gives 77% purity with 82% efficiency (compare Table 1 for the same strategy with single-tagging).

(7) These double-tagged results are nonetheless quite far from perfect, showing that gluon identification is only one part of the problem. Detector resolution is responsible for essentially all the misreconstructions in the double-tagged case, and must be a major factor in the single-tagged case too. Better resolution would allow better reconstruction.

Acknowledgments

We thank Erwin Mirkes and Tim Stelzer for discussions. RJNP thanks the University of Wisconsin for hospitality during part of this work. VB thanks the Institute for Theoretical Physics at the University of California, Santa Barbara for hospitality during part of this work. This research was supported in part by the U.S. Department of Energy under Grants No. DE-FG02-95ER40896 and No. DE-FG02-84ER40173, in part by the National Science Foundation under Grant No. PHY94-07194, in part by the University of Wisconsin Research Committee with funds granted by the Wisconsin Alumni Research Foundation and in part by Conselho Nacional de Desenvolvimento Científico e Tecnológico (CNPq).

References

- [1] CDF collaboration, F. Abe *et al.*, Phys. Rev. Lett. **73**, 225 (1994); **74**, 2626 (1995); Phys. Rev. **D50**, 2966 (1994); **D51**, 4623 (1995); **D52**, 2605 (1995); FERMILAB-PUB-95/149-E.
- [2] D0 collaboration, S. Abachi *et al.*, Phys. Rev. Lett. **74**, 2632 (1995); Phys. Rev. **D52**, 4877 (1995).
- [3] F.A. Berends, W.T. Giele and H. Kuijf, Nucl. Phys. **B321**, 39 (1989); F.A. Berends, W.T. Giele, H. Kuijf and B. Tausk, *ibid.* **B357**, 32 (1991).
- [4] L.H. Orr, T. Stelzer and W.J. Stirling, Phys. Rev. **D52**, 124 (1995).
- [5] T. Stelzer and W.F. Long, Comput. Phys. Commun. **81**, 357 (1991).
- [6] R.K. Ellis and J.C. Sexton, Nuc. Phys. **B282**, 642 (1987).
- [7] V. Barger, E. Mirkes, R.J.N. Phillips, T. Stelzer, Phys. Lett. **B338** (1994) 336; V. Barger, E. Mirkes, J. Ohnemus, R.J.N. Phillips, *ibid.* **B344** (1994) 329.

Figure Captions

1. Typical Feynman diagrams for $t\bar{t}$ production and decay with an extra gluon, at the Tevatron.
2. Distributions versus gluon transverse momentum for true unsmeared events (solid histograms) and reconstructed smeared events with a single b -tag (dashed histograms), using our basic reconstruction procedure;(a) Class A, (b) Class B, and (c) Class C.
3. Dependence on the separation $\Delta R(gb)$ for (a) Class B and (b) Class C events. Solid (dashed) histograms denote true (basic-reconstructed) events.
4. Dependence on the gluon energy $E(g)$ in the parent top rest-frame for (a) Class B and (b) Class C events. Solid (dashed) histograms denote true (basic-reconstructed) events.
5. Dependence on the separation $\Delta R(gb)$ for (a) Class B and (b) Class C events. Solid (dashed) histograms denote true (refined-reconstructed) events. The compromise reconstruction method also gives the dashed curves.

Figure 1

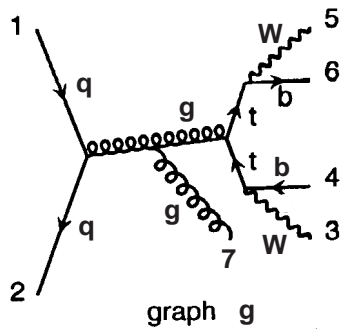
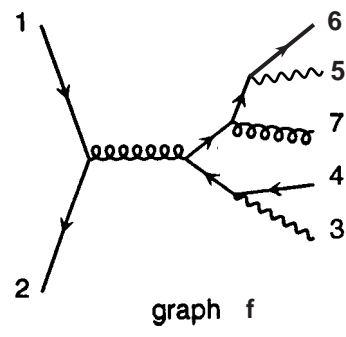
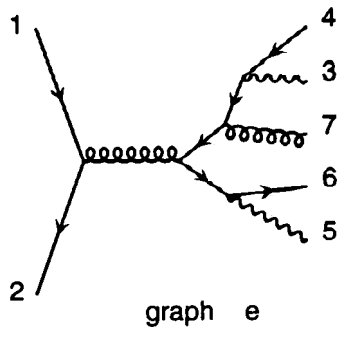
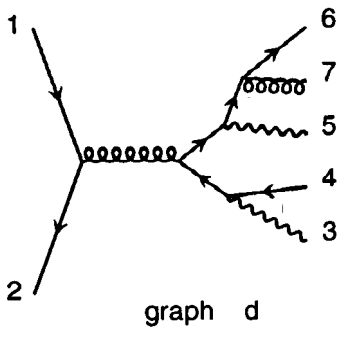
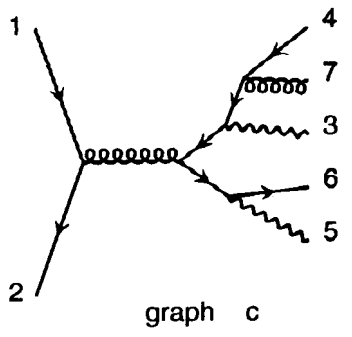
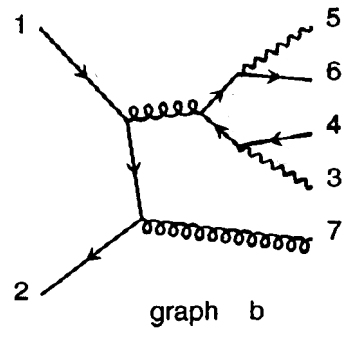
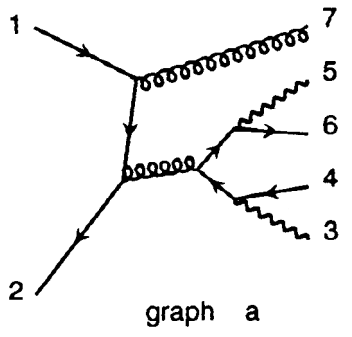


Figure 2

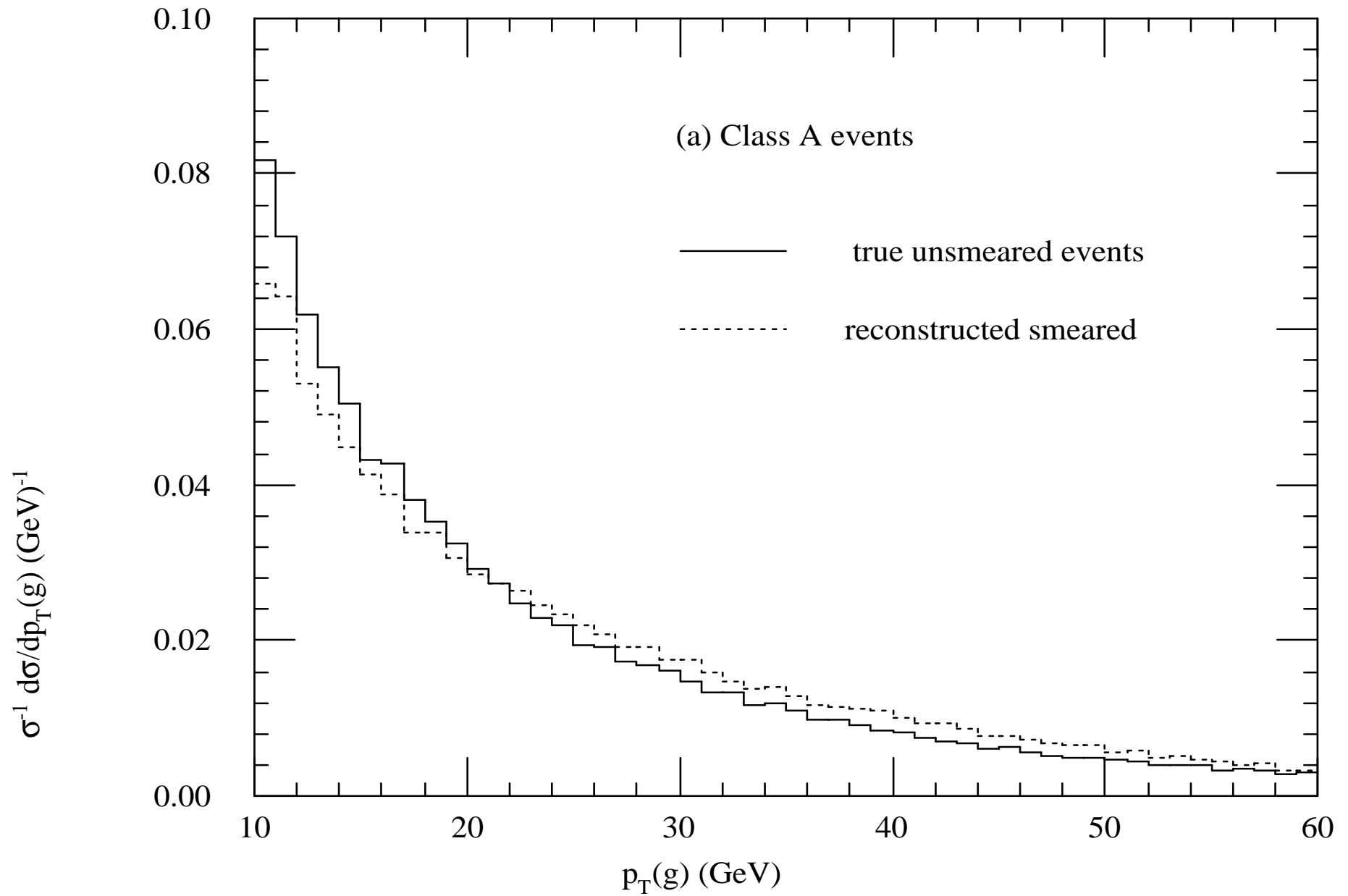


Figure2

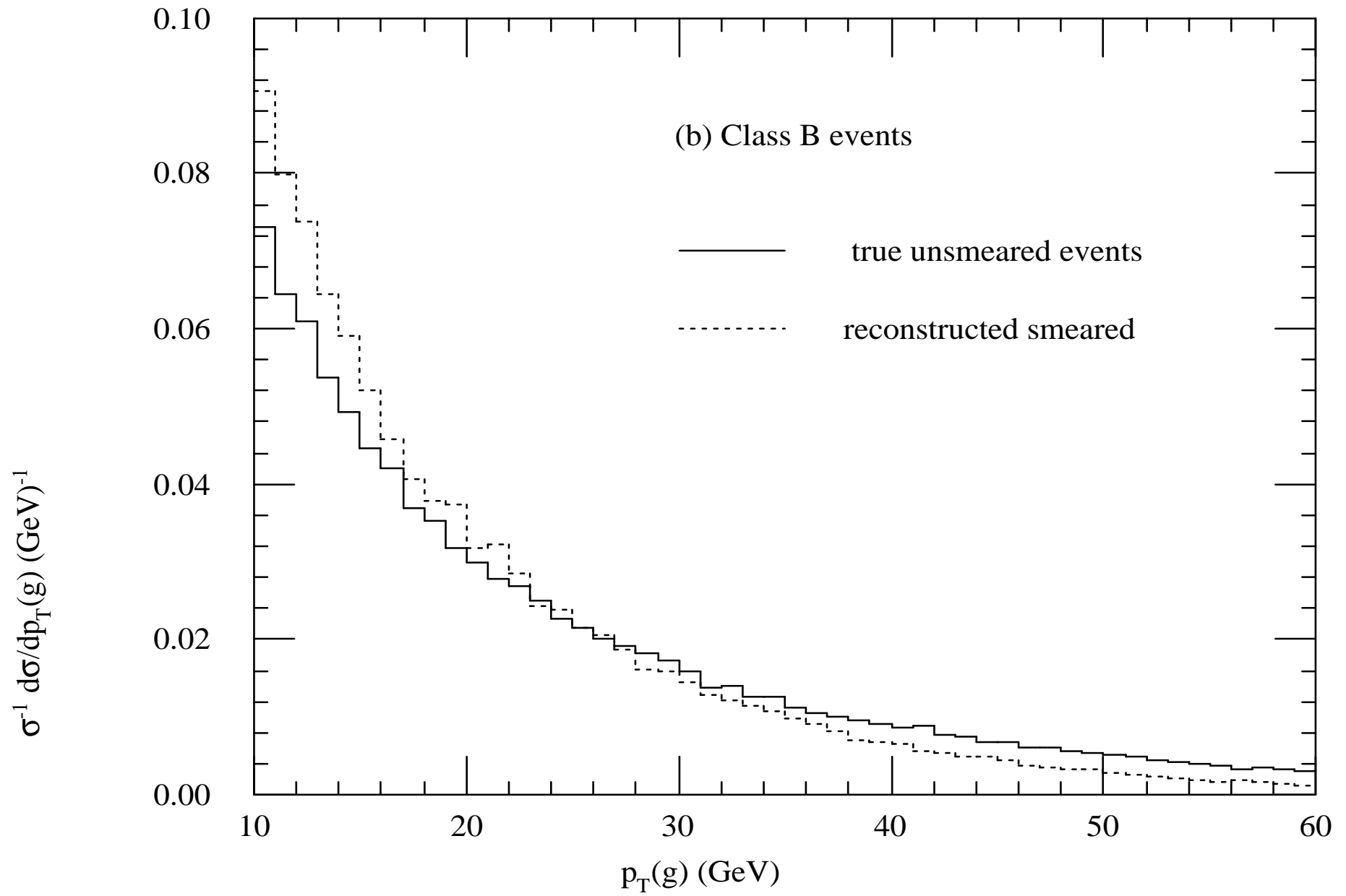


Figure 2

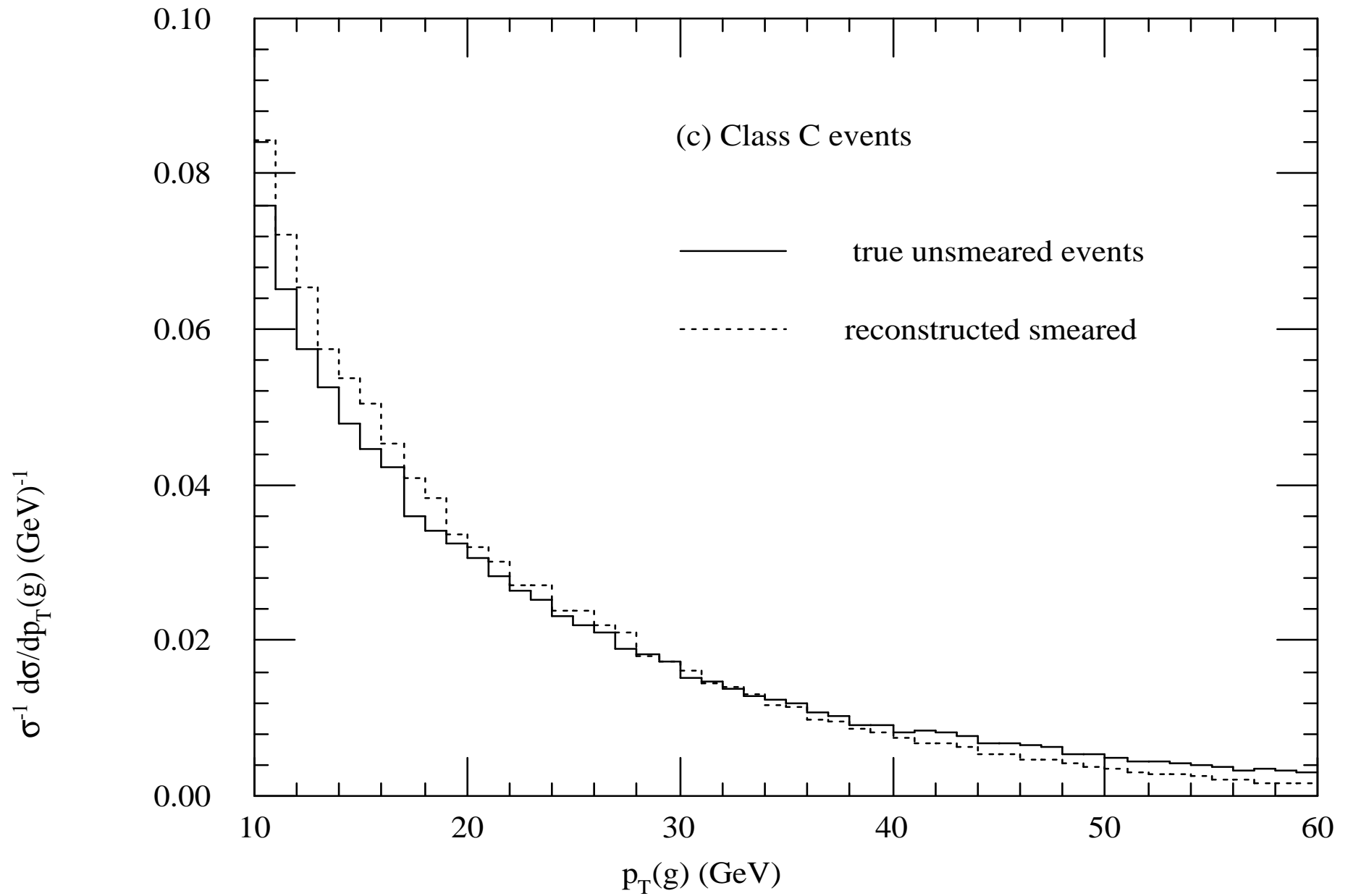


Figure 3

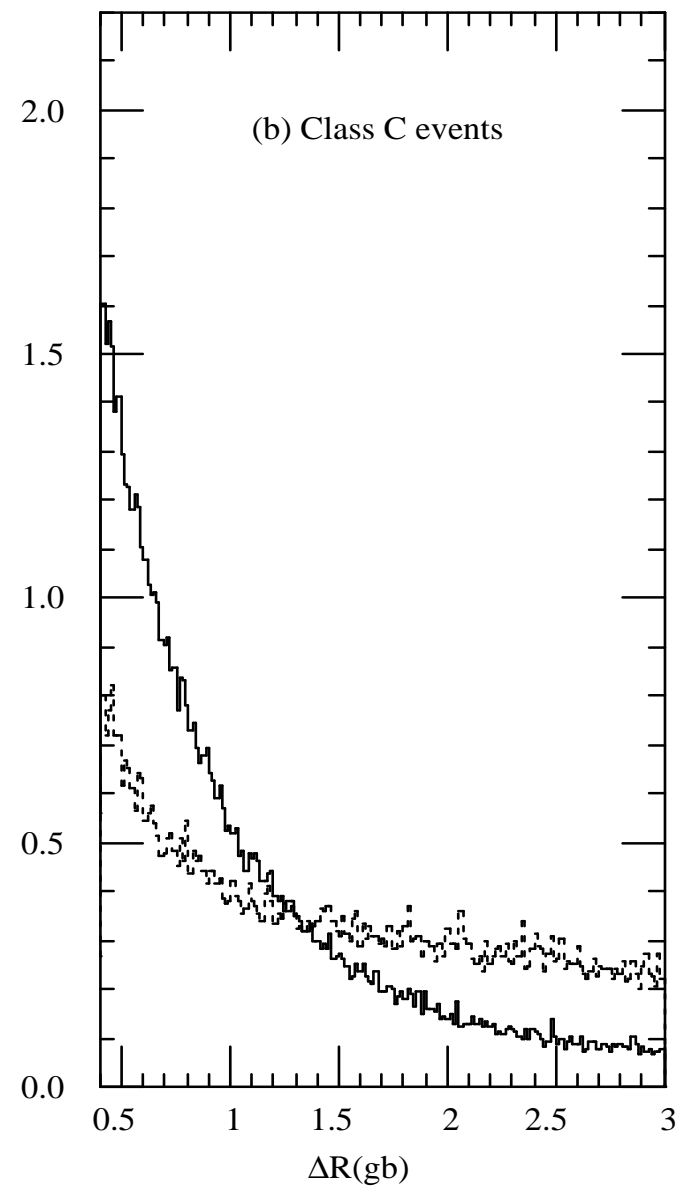
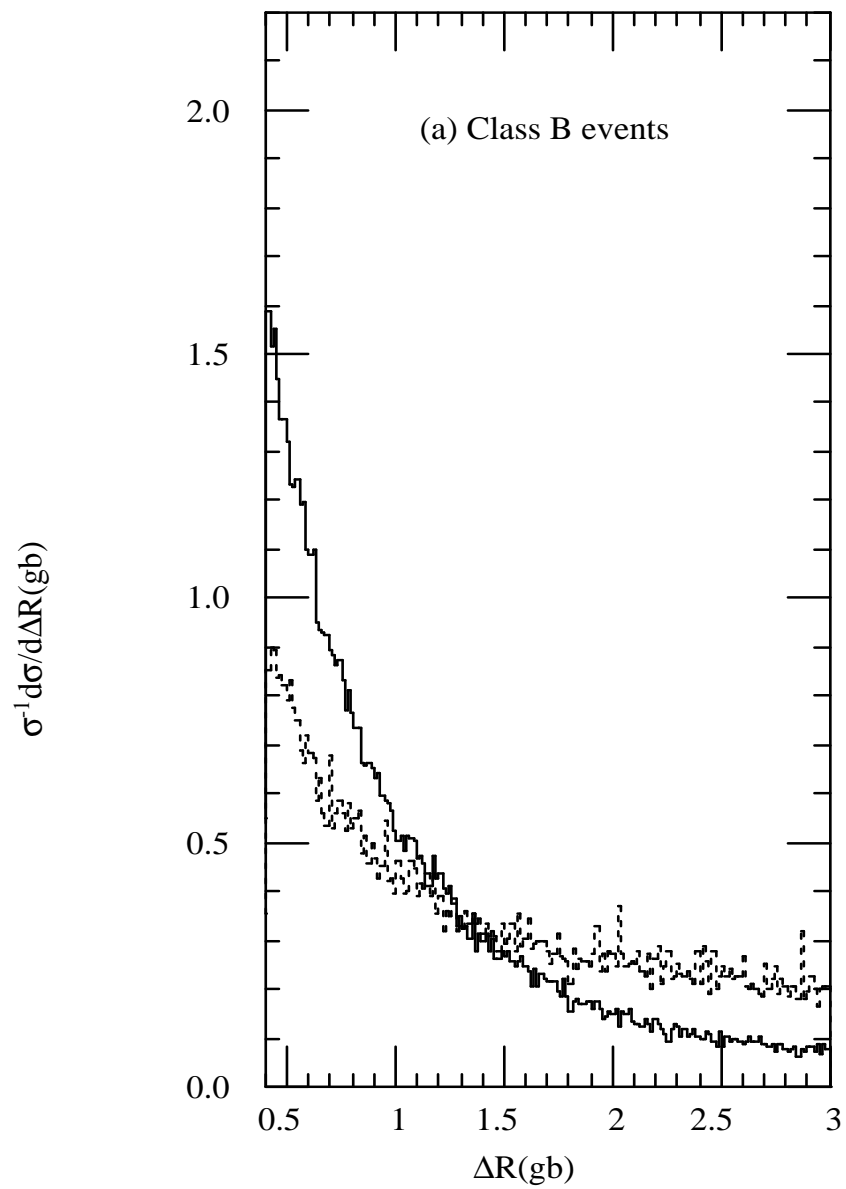


Figure 4

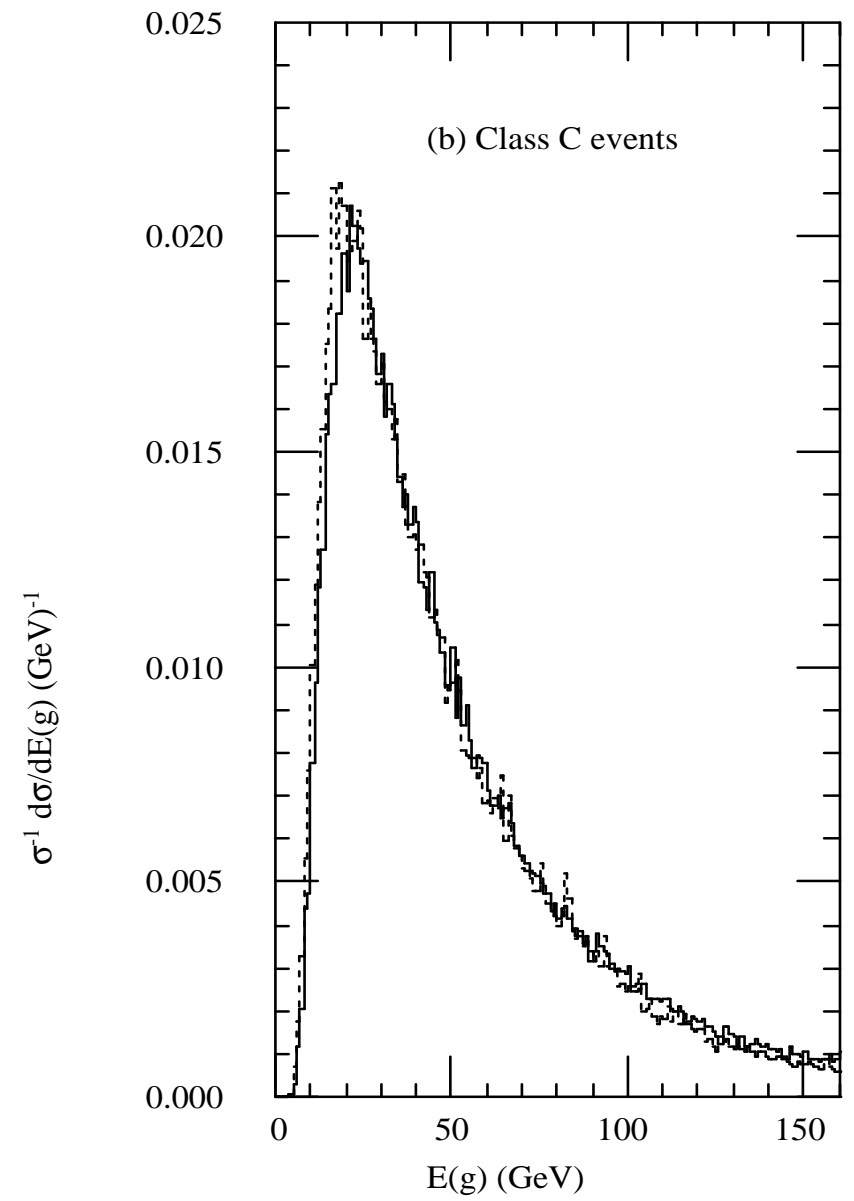
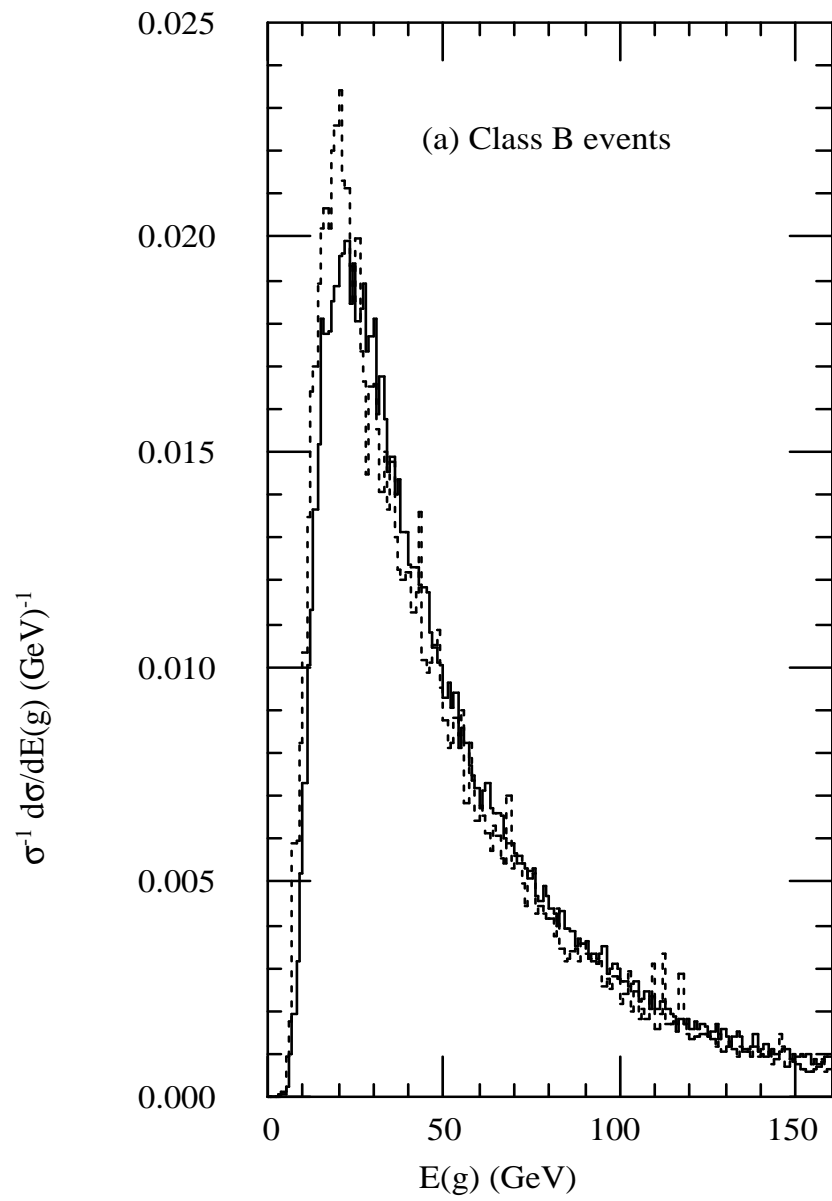


Figure 5

